HHS Public Access

Author manuscript

Adv Funct Mater. Author manuscript; available in PMC 2024 August 01.

Published in final edited form as:

Adv Funct Mater. 2023 August 01; 33(31): . doi:10.1002/adfm.202213368.

Hybrid Shear-thinning Hydrogel Integrating Hyaluronic Acid with ROS-Responsive Nanoparticles

Mariah G. Bezold,

Andrew R. Hanna,

Bryan R. Dollinger,

Prarthana Patil,

Fang Yu,

Craig L. Duvall[*], **Mukesh K. Gupta**[*]

Department of Biomedical Engineering, Vanderbilt University, Nashville, TN 37235 USA

Abstract

Nanoparticle (NP) supra-assembly offers unique opportunities to tune macroscopic hydrogels' mechanical strength, material degradation, and drug delivery properties. Here, synthetic, reactive oxygen species (ROS)-responsive NPs are physically crosslinked with hyaluronic acid (HA) through guest-host chemistry to create shear-thinning NP/HA hydrogels. A library of triblock copolymers composed of poly(propylene sulfide)-*bl*-poly(N,N-dimethylacrylamide)-*bl*-poly(N,N-dimethylacrylamide-*co*-N-(1-adamantyl)acrylamide) are synthesized with varied triblock architectures and adamantane grafting densities and then self-assembled into NPs displaying adamantane on their corona. Self-assembled NPs are mixed with β-cyclodextrin grafted HA to yield eighteen NP/HA hydrogel formulations. The NP/HA hydrogel platform demonstrates superior mechanical strength to HA-only hydrogels, susceptibility to oxidative/enzymatic degradation, and inherent cell-protective, antioxidant function. The performance of NP/HA hydrogels is shown to be affected by triblock architecture, guest/host grafting densities, and HA composition. In particular, the length of the hydrophilic second block and adamantane grafting density of self-assembled NPs significantly impacts hydrogel mechanical properties and shear-thinning behavior, while ROS-reactivity of poly(propylene sulfide) protects cells from cytotoxic ROS and reduces oxidative degradation of HA compared to HA-only hydrogels. This work provides insight into polymer structure-function considerations for designing hybrid NP/HA hydrogels and identifies antioxidant, shear-thinning hydrogels as promising injectable delivery platforms for small molecule drugs and therapeutic cells.

Graphical Abstract

[*] mukesh.k.gupta@vanderbilt.edu, craig.duvall@vanderbilt.edu.

Supporting Information

Supporting Information is available from the Wiley Online Library or from the author.

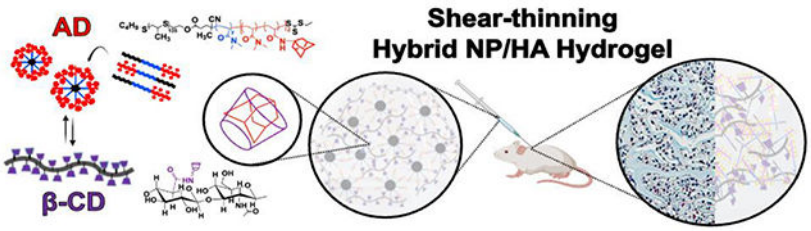

Shear-thinning hydrogels are assembled through physical crosslinking mediated by guest-host complexation between adamantane and β-cyclodextrin macromers in order to integrate synthetic nanoparticles and hyaluronic acid into a single hybrid NP/HA hydrogel system which allows for injectable delivery and local retention of small molecule drugs and therapeutic cells in tissue engineering applications.

Keywords

shear-thinning hydrogels; triblock copolymer nanoparticles; reactive oxygen species (ROS) responsive polymer; hyaluronic acid; guest-host chemistry

1. Introduction

Hydrogels have been successfully applied as biomaterial platforms for drug and cell delivery[1] across various tissue reparative applications, as they offer the capability to be chemically optimized for injectability and for tight control over properties of the hydrogel matrix such as pore structure[2], degradation mechanisms[3], and mechanical properties[3, 4]. While covalently crosslinked hydrogels are ideal for applications that demand high mechanical integrity[5], injectable hydrogels are more readily achieved using physical crosslinking through intermolecular hydrogen bonding[6], hydrophobic interactions[7], chain entanglement[8], or electrostatic interactions[9].

We previously developed a physically crosslinked injectable hydrogel based on the thermal gelation of the synthetic polymer PNIPAAM[10]. This system was based on nanoparticles (NPs) self-assembled from ABC triblock copolymers of the form poly(propylene sulfide)-*block*-poly(*N,N*-dimethylacrylamide)-*block*-poly(*N*-isopropylacrylamide) (PPS-*b*-PDMA-*b*-PNIPAAM) (PDN). PPS serves as the core-forming component which allows for loading of small-molecule drugs. The oxidation of PPS by reactive oxygen species (ROS) converts the core of the self-assembled NPs from hydrophobic to hydrophilic, providing this hydrogel with antioxidant function as well as ROS-responsive degradation and drug release mechanisms as a function of PPS[11, 12]. The PDN hydrogels were shown to protect various cell types, including fibroblasts, mesenchymal stromal cells (MSCs), and pancreatic islet organoids, from cytotoxic levels of ROS[10, 13, 14]. Furthermore, supplementing PDN hydrogels with type I collagen improved the adhesion and spreading of 3D encapsulated cells[13].

In recent years, other NP-based hydrogels have been developed to enable injectability through physical crosslinking mediated by reversible, hydrophobic interactions between

polyester NPs and biopolymer derivatives[15, 16]. These shear-thinning hydrogels demonstrate a decrease in their storage modulus in response to shear stress, allowing them to be injected through a needle or catheter. Since shear-thinning hydrogels are based on physical interactions which reform rapidly after the removal of shear stress, these materials also display self-healing behavior. A combination of shear-thinning and self-healing behavior allows for non-invasive injection and local retention of these materials post-injection, which are desirable behaviors for local delivery of therapeutic small molecule drugs or stem cells[17, 18].

The objective of this work was to develop ROS-responsive, shear-thinning hydrogels as an injectable delivery platform that harnesses the desirable features of the previous PDN system while utilizing a shear-thinning gelation mechanism based on physical crosslinking between NPs self-assembled from PPS triblock copolymers and the biologically-active polymer hyaluronic acid (HA). These features allow for easier handling under ambient conditions and eliminate the potential for forming non-resorbable, hydrophobic aggregates of PNIPAAM when delivered *in vivo*. The gelation mechanism of the proposed system relies on guest-host interactions between β-cyclodextrin (CD) and adamantane (AD), which facilitate physical crosslinking between two hydrogel components. The host molecule, CD, is a cone-shaped cyclic oligosaccharide that possesses a hydrophobic interior cavity that forms inclusion complexes with small hydrophobic guest molecules such as AD[19]—mixing individual polymer components functionalized with either CD or AD yields shear-thinning hydrogels due to the reversible interactions between the guest-host complexes. Previous work has explored HA-only shear-thinning hydrogels based on guest-host interactions for many applications, including the delivery of therapeutic stem cells for tissue repair and regeneration[17, 20–22].

The shear-thinning hydrogel reported in the studies below relies on guest-host interactions between CD grafted onto HA and AD grafted onto third block, forming the corona of NPs self-assembled from PPS triblock copolymers. This hybrid NP/HA composition integrates ROS-responsive chemistry, allows for susceptibility to both oxidative and enzymatic degradation, and incorporates the natural bioactivity of HA, a native extracellular matrix (ECM) molecule that is used in wound dressings such as Hyalofill[23]. To elucidate the structure-function relationships of this hybrid design, a library of ABC triblock PPS-*b*-PDMA-*b*-P(DMA-*co*-ADA) copolymers with varying degrees of polymerization (DPs) of the DMA block and different densities of AD on the third P(DMA-*co*-ADA) block was synthesized. Rheology was used to identify NP/HA hydrogels with increased mechanical strength and desirable shear-thinning behavior, and four lead candidate NP/HA hydrogels were further characterized *in vitro* for injectability, small molecule drug loading and release, susceptibility to oxidative and enzymatic degradation, cytocompatibility, cell encapsulation and protection from cytotoxic ROS, as well as *in vivo* for cellular infiltration and resorption relative to HA-only hydrogels.

2. Results and Discussion

2.1. Synthesis of ABC Triblock Copolymers Grafted with Guest Molecule (AD)

A library of ABC triblock polymers of poly(propylene sulfide)-b-poly(N,N-dimethylacrylamide)-b-poly(N,N-dimethylacrylamide-co-N-(1-adamantyl)acrylamide) was successfully synthesized with varied DP of the second PDMA block and varied grafting percent of AD in the third block (Figure 1A–B). The variations in PDMA length (B block) and AD grafting density in the third block (C block) of triblock copolymers were explored to understand the synergistic impact of the hydrophilic "linker block" length and the density of the hydrophobic AD guest molecule on ability of triblock copolymers to form NPs that can effectively engage with HA-CD to form shear-thinning hydrogels. For the triblock copolymers, poly(propylene sulfide) with a hydroxyl terminus (PPS_{135}-OH) was synthesized by anionic polymerization and confirmed by characteristic peaks in ^{1}H NMR spectra. PPS_{135}-OH was conjugated to the chain transfer agent (CTA) 4-cyano-4-(ethylsulfanylthiocarbonyl) sulfanylpentanoic acid (ECT) so that the addition of the second and third blocks could be accomplished by reversible addition-fragmentation chain transfer (RAFT) polymerization (Figure 1A). Three diblock copolymers, each with a different DP (150, 200, and 300), were prepared by RAFT polymerization of the hydrophilic monomer DMA and characterized by ^{1}H NMR spectra. Gel permeation chromatography (GPC) confirmed the formation of unimodal diblock copolymers with varied DMA block lengths (Figure 1C–E).

Each diblock copolymer was then used to prepare two different triblock copolymers with either 10% or 20% grafting density of AD through RAFT copolymerization of DMA and N-(1-adamantyl)acrylamide (ADA) (Figure S1–2, SI File) while maintaining a constant DP of 200 for the third block. Synthesis of ABC triblock copolymers with 30% grafting density of AD resulted in the final composition precipitating during self-assembly of NPs due to destabilization effect of the hydrophobic of AD molecules (not shown); therefore, the grafting density of AD for triblock copolymers was limited to 20% to ensure that the final triblock copolymers maintained sufficient stability in aqueous solutions. GPC chromatograms indicated successful addition of the third block to each diblock copolymer, confirming the successful creation of the final triblock copolymers which are denoted as D_x-AD_y where *x* represents the DP for the PDMA block, and *y* represents the grafting density of AD on the third block (Figure 1C–E). The chemical structure and block length of each triblock copolymer was confirmed by ^{1}H NMR spectra (representative spectra for PPS D_{150}-$AD_{10\%}$ and PPS D_{150}-$AD_{20\%}$ shown in Figure S3, SI File). Therefore, a combination of ^{1}H NMR spectroscopy and GPC validated the combined anionic and RAFT polymerization approach for preparing multi-functional triblock polymers while carefully controlling the variation in block size and AD grafting density.

2.2. Characterization of Self-Assembled Nanoparticles Grafted with Host Macromer (AD)

Dynamic light scattering (DLS) analysis and cryogenic transmission electron microscopy (cryo-TEM) were utilized to characterize the size and morphology of ABC triblock copolymers self-assembled into NPs in aqueous solution. DLS measurements (Figure 1F) (1 mg/mL PBS) indicated that self-assembled NPs composed of triblock copolymers grafted

with 10% AD were stable and showed no aggregation. Self-assembled NPs grafted with a higher grafting density of 20% AD demonstrated aggregation for those composed of triblock copolymers containing shorter PDMA blocks with DPs of 150 and 200; however, self-assembled NPs composed of triblock copolymers with longer PDMA blocks with a DP of 300 were able to be grafted with 20% AD and still form small, uniform NPs. The polydispersity indices (PDI) from DLS further confirmed these trends, with triblock copolymers containing shorter PDMA blocks resulting in self-assembled NPs with greater PDI (Figure S4, SI File). These results suggest that the hydrophilic PDMA block plays an important role in solubilizing the third block grafted with the hydrophobic AD guest molecule. The NP morphology obtained from cryo-TEM imaging further supports these quantitative measurements obtained from DLS and illustrates the formation of uniform spherical NPs (Figure 1G and Figure S5, SI File).

2.3. Modularity of Formulation Allows NP/HA Hydrogel System to Achieve a Range of Mechanical Properties with Shear-thinning Behavior

Rheological characterization was performed on a library of eighteen different NP/HA hydrogel formulations to identify those which exhibit sufficient mechanical strength, possessing a storage modulus (G′) of at least 1000 Pa and demonstrate desirable shear-thinning and self-healing behavior, with a yield strain of at least 100%[22, 24]. A library of hyaluronic acid grafted with CD (HA-CD) polymers was created by varying the grafting density of CD on the native HA biopolymer (Figure S6, SI File) in order to determine an optimum grafting density of CD on HA polymer which would allow for the formation of stable NP/HA shear-thinning hydrogels when mixed with NPs self-assembled from candidate triblock copolymers. The PPS D_{150}-$AD_{10\%}$ triblock copolymer was selected for initial screening with HA-CD polymers of varying CD grafting densities as this copolymer formed stable, uniform NPs, and the block lengths of this triblock copolymer approximately matched those used in previously described thermoresponsive hydrogels[11]. The NP/HA hydrogels were formulated by mixing D_{150}-$AD_{10\%}$ NPs with HA-CD_x polymers containing 10%, 20%, or 34% grafting of CD, where grafting of CD on HA was confirmed by characteristic peaks in ^{1}H NMR spectra (Figure S7, SI File). All NP/HA hydrogels formed visible hydrogels through guest-host inclusion complexes, as confirmed by vial inversion (Figure S8A, SI File). Rheometry were performed on each NP/HA hydrogel and revealed that G′ of each NP/HA hydrogel increased when the grafting density of CD increased from 10% to 20%; however, G′ was observed to decrease when the grafting density of CD was further increased to 34% (Figure S8B, SI File). The decrease in G′ observed for HA-$CD_{34\%}$ is likely due to its reduced solubility, increased viscosity, and the steric hindrance between closely-packed CD molecules, all of which contribute to impaired mixing of components and reduced guest-host complex formation between CD and AD[21]. Therefore, HA-$CD_{20\%}$ was selected as Component B to investigate further mechanical properties of various NP/HA hydrogels formed with different ABC triblock copolymers. Analogous HA polymers grafted with the guest molecule (HA-$AD_{20\%}$) were also synthesized with a grafting density of 20% AD and confirmed by ^{1}H NMR spectra (Figure S9 and S10, SI File) to create conventional HA-only shear-thinning hydrogels as a control hydrogel for comparison to hybrid NP/HA hydrogel systems.

To further characterize guest-host interactions between AD-functional self-assembled NPs and HA-$CD_{20\%}$, DLS measurements were performed when either HA-$CD_{20\%}$ or unmodified HA was mixed with PPS D_{150}-$AD_{10\%}$ NPs in dilute solutions. Increased size and PDI was observed when HA-$CD_{20\%}$ was mixed with PPS D_{150}-$AD_{10\%}$ NPs, suggesting interactions between HA-$CD_{20\%}$ and the self-assembled NPs; however, no significant increases in size or PDI were observed when unmodified HA was mixed with PPS D_{150}-$AD_{10\%}$ NPs (Figure S11, SI File). Cryo-TEM images of PPS D_{150}-$AD_{10\%}$ NPs mixed with HA-$CD_{20\%}$ further support aggregation between NPs and HA, presumably driven by guest-host pairing (Figure 2A and Figure S12, SI File). Cryogenic scanning electron microscopy (cryo-SEM) was also performed to visualize hydrated NP/HA hydrogels and observe the porous microstructure (Figure 2B). The average pore size of the NP/HA hydrogel network (0.75 microns) determined from cryo-SEM was smaller compared to the average pore size of control HA-only shear-thinning hydrogels (1.5 microns) (Figure S13, SI File), which is most likely a consequence of the more organized double network structure of NP/HA hydrogels[25].

Prior to mechanical analysis of a full library of NP/HA hydrogels composed from candidate PPS triblock copolymers, the initial PPS D_{150}-$AD_{10\%}$ NP/HA hydrogel formulation was assessed by rheometry to confirm shear-thinning and self-healing behavior based on guest-host mediated physical crosslinking. Frequency sweep measurements demonstrated that this NP/HA hydrogel maintained a higher G' than loss modulus (G'') when subjected to a wide range of frequencies from 0.1 to 100 Hz (Figure S14A, SI File). Percent strain sweep measurements revealed that the NP/HA hydrogel exhibited gel behavior ($G' > G''$) over a broad range but illustrated a transition ($G' < G''$) to a viscous liquid at strains over 80% (Figure S14B, SI File). Stepwise percent strain-based time sweep measurements indicated that G' of the NP/HA hydrogel recovered rapidly and completely throughout repeated cycles of high (300%) and low strain (0.5%), confirming the reversibility of guest-host pair-based physical crosslinking and self-healing behavior of NP/HA hydrogels (Figure 2C). Shear-thinning and self-healing behavior of the NP/HA hydrogel were further confirmed through continuous flow measurements where hydrogel viscosity was observed to decrease with increasing shear rate but rapidly recovered when shear rate was reduced (Figure 2D).

A more comprehensive range of candidate NP/HA hydrogels composed of NPs self-assembled by PPS triblock copolymers of varying block structure and grafting density were characterized by rheometry to identify lead candidate NP/HA hydrogels with optimum mechanical integrity and desirable shear-thinning behavior (Figure 2E–K). The nomenclature of each candidate NP/HA hydrogel was defined based on ABC triblock copolymer composition and the stoichiometric ratio of CD/AD at which the NP/HA hydrogel was formed. For example, NP/HA hydrogels formulated with PPS D_{150}-$AD_{10\%}$ self-assembled NPs and HA-$CD_{20\%}$ mixed at a ratio of 1CD/1AD was denoted as D_{150}-$AD_{10\%}$ 1CD/1AD. Stepwise cyclic percent strain time sweep measurements were performed on each NP/HA hydrogel to assess the effects of the PDMA block length, the stoichiometric ratio of CD/AD, and the AD grafting density of the third block on resulting hydrogel's mechanical strength and shear-thinning behavior, where mechanical strength was assessed by G' and shear-thinning behavior was assessed by tanδ. Every NP/HA hydrogel formulation across the entire library of formulations tested consistently yielded solid hydrogels with shear-thinning behavior. The tanδ (ratio of G''/G') values calculated

for each NP/HA hydrogel at both high (300%) and low strain (0.5%) are represented in the heat map in Figure 2E. All NP/HA hydrogel formulations possessed tanδ values less than 1 at 0.5% strain, indicating elastic solid-like mechanical behavior, but possessed tanδ values greater than 1 at 300% strain, indicating viscous liquid-like behavior.

While all formulations consistently formed NP/HA hydrogels possessing shear-thinning behavior, there were trends that emerged regarding the effect of PDMA block length and grafting density of AD on the mechanical strength of the resulting NP/HA hydrogels (Figure 2F–K). Triblock copolymers with PDMA blocks with a DP of 150, and 10% grafting of AD in the third block yielded hydrogels with higher G′ (D_{150}-$AD_{10\%}$ 1CD/1AD) compared to those hydrogels composed of triblock copolymers with the same PDMA block length but increased grafting density of 20% AD in the third block (D_{150}-$AD_{20\%}$ 1CD/1AD) (Figure 2F). However, when the PDMA block DP was increased to 200 or 300, the hydrogels containing NPs made from these triblock copolymers grafted with 20% AD in the third block yielded higher G′ compared to hydrogels composed with triblock copolymers with the same PDMA block length and 10% grafting of AD (Figure 2G–H). These results suggest that increased guest-host interactions as a result of higher AD density in the third block is only realized when the triblock copolymer contains a PDMA block long enough to solubilize the hydrophobic third block grafted with a higher density of AD which may otherwise tend to self-aggregate or form a flower-like micelle structure.

Next, a range of NP/HA hydrogels were prepared at different stoichiometric ratios of CD to AD to evaluate the effect of guest-host interactions when one component is more than the other (Figure 2I–K). The NP/HA hydrogels formed at the ratios of 1CD/1AD and 2CD/1AD resulted in higher G′ compared to analogous NP/HA hydrogels formed at a ratio of 1CD/2AD. Among the NP/HA hydrogels formed at 1CD/1AD and 2CD/1AD ratios, those containing longer PDMA blocks tended to correlate with increased G′ for the NP/HA hydrogel. Effective recovery (> 95%) of G′ was also confirmed for all NP/HA hydrogel formulations over five repeated step-strain measurements, which confirms that the hybrid NP/HA hydrogel system provides self-healing behavior over a broad range of formulation conditions (Figure S15, SI File).

Based on this robust rheological characterization, hydrogels based on the triblock copolymers PPS D_{150}-$AD_{10\%}$ and PPS D_{300}-$AD_{20\%}$ were chosen for further *in vivo* and *in vitro* characterization. These two PPS triblock copolymers demonstrated consistent and stable NP formation and yielded NP/HA hydrogel formulations with excellent shear-thinning properties. However, these two NP/HA hydrogel formulations showed significantly different storage moduli due to their distinct DMA block lengths and AD grafting densities. Therefore, these hydrogels were chosen to assess triblock architecture's effect on mechanical properties for two NP/HA hydrogel formulations that display idealized shear-thinning behavior.

To demonstrate the universality of the NP/HA hydrogel system and to generate a non-ROS-responsive control NP, a PCL-based D_{300}-$AD_{20\%}$ triblock copolymer (Figure S16, SI File) was synthesized as an analog of PPS D_{300}-$AD_{20\%}$. The PCL-based triblock copolymer structure and grafting density of AD was confirmed by ^{1}H NMR spectra (Figure S17, SI

File), and the self-assembly of PCL-based triblock copolymers into small, uniform NPs was confirmed by DLS and cryo-TEM (Figure S18A–B, SI File). The PCL NPs formed NP/HA hydrogels when mixed with HA-$CD_{20\%}$ and possessed similar structure to the analoguos PPS NP/HA hydrogels as observed by cryo-TEM of both PPS-based and PCL-based D_{300}-$AD_{20\%}$ 1CD/1AD hydrogels (Figure S19A–B, SI File). Conventional HA-only shear-thinning hydrogels, where HA-$AD_{20\%}$ was substituted in place of the NP component, were also formed to create control HA/HA hydrogels.

Additional frequency, time, and strain sweep rheological measurements were performed on four lead candidate PPS NP/HA hydrogels as well as both the control PCL NP/HA and HA/HA hydrogels. The two candidate PPS triblock copolymers, D_{150}-$AD_{10\%}$ and D_{300}-$AD_{20\%}$, were mixed with HA-$CD_{20\%}$ at two different stoichiometric ratios of CD to AD (1CD/1AD and 2CD/1AD) to yield four lead candidate PPS NP/HA hydrogels for these measurements to evaluate how increased HA content relative to the synthetic NP in NP/HA hydrogels impacts the *in vitro* and *in vivo* degradation profile of NP/HA hydrogels. These measurements revealed that all four candidate PPS NP/HA hydrogels and both control hydrogels demonstrated shear-thinning and self-healing behavior and confirmed that PPS NP/HA hydrogel formulation at 1CD/1AD or 2CD/AD ratio did not alter mechanical behavior (Figure S20, SI File). The effect of overall weight percent in NP/HA hydrogels was also evaluated by performed rheometry on one lead candidate PPS NP/HA hydrogel (D_{300}-$AD_{20\%}$ 1CD/1AD) formed at 5 wt%, 7.5 wt%, and 10 wt% (Figure S21, SI File). As expected, the G′ of PPS NP/HA hydrogels correlated with increasing polymer concentration, but all hydrogels still retained shear-thinning behavior as observed by stepwise percent strain-based time sweep measurements. Furthermore, frequency sweeps demostrated hydrogels undergo transition from viscous (liquid) to elastic (solid) phase with increasing frequencies due to a progressive decrease in relaxation time that favors the elastic properties (G') over viscous properties (G'') towards the higher frequencies[20] . Similar mechanical analysis was performed on the same PPS NP/HA hydrogel when its temperature increased from 25°C to 45°C, demonstrating that hydrogels maintained consistent mechanical properties at the physiological temperature of 37°C (Figure S22A, SI File). A final rheological analysis was performed to study the effect of increasing strain on candidate PPS NP/HA and control PCL NP/HA hydrogels. Both PPS-based and PCL-based D_{300}-$AD_{20\%}$ 1CD/1AD hydrogels were subjected to time sweep measurements performed at constant low 0.5% strain with successively increasing high strains of 300%, 400%, and 500%. Both hydrogels demonstrated increasing shear-thinning behavior when subjected to increasing high strains but immediately recovered their initial G′ once high strain was removed (Figure S22B–C, SI File). Rapid and complete recovery of mechanical properties following high strain suggests that NP/HA hydrogels can form stable hydrogels following injection and dilution *in vivo*. This behavior was further visualized during injection of Nile red loaded PPS D_{150}-$AD_{10\%}$ NP/HA 1CD/1AD hydrogels through a 30G needle and directly into PBS (Figure 3A) where the hydrogel retained its mechanical integrity following injection and dilution in PBS (Figure 3B and Supporting Video File, SV File).

2.4. PPS-based NP/HA Hydrogels Provide an Injectable Delivery Platform for Therapeutic Cells

To establish the clinical potential of NP/HA hydrogels as an injectable platform, the force required for injection of two candidate PPS NP/HA hydrogels as well as the control HA/HA hydrogel was measured with respect to needle gauge, needle length, and polymer concentration. Representative traces of force over the time were recorded during hydrogel injection through needles of three different gauges and two different lengths (Figure 3C–E), and the injection force was reported as the value recorded when the trace reached a plateau (Figure 3F–H). The force required to inject PPS D_{300}-$AD_{20\%}$ 1CD/1AD hydrogels through a 25G needle exceeded the maximum force of the load cell, and therefore, injection force was recorded as the maximum force reached during injection force measurement for this hydrogel. Injection force for all hydrogels correlated increasing needle gauge and increasing needle length. However, the force required for injection for PPS NP/HA hydrogels was higher than control HA/HA hydrogels, which is due to the higher moduli reported for candidate NP/HA hydrogels from previous rheological measurements above. Injection forces were also measured when candidate PPS D_{300}-$AD_{20\%}$ NP/HA 1CD/1AD hydrogel was formed at increasing weight percent, and as expected, hydrogels required increasing injection force when formed at increasing weight percent (Figure S23, SI File). Collectively, these data confirm that the forces needed for the injection of PPS NP/HA hydrogels in any formulation were significantly lower than forces (20-80 N) reported as acceptable for clinical administration[26].

The candidate NP/HA hydrogels were also evaluated to demonstrate their ability to protect cells from shear stress during their administration through a needle. A 22G needle (0.25 inch length) was used for these studies since injection of both candidates PPS NP/HA hydrogels using this needle required a force between 5 to 7 N, which falls within the range reported for successful injection of viable cells within HA-only hydrogels[20]. After mMSCs were suspended within the two candidate PPS NP/HA hydrogels (D_{150}-$AD_{10\%}$ 1CD/1AD and D_{300}-$AD_{20\%}$ 1CD/1AD), each hydrogel was loaded into a sterile syringe, and 25 μL of each hydrogel was injected at a constant flowrate of 2 mL/h into the wells of a 96-well plate (Figure 3I). The viability of mMSCs post-injection was significantly higher when either candidate PPS NP/HA hydrogel was used for injection of mMSCs compared to when mMSCs were injected in PBS alone (Figure 3J).

2.5. PPS-based Nanoparticles Allow for Small Molecule Drug Loading and Oxidative Release from NP/HA Hydrogels

To characterize small molecule drug loading, Nile red was loaded into PPS and PCL NPs at a range of Nile red to polymer weight ratios. The two lead candidate PPS triblock copolymers, D_{150}-$AD_{10\%}$ and D_{300}-$AD_{20\%}$, loaded up to ~150 μg of Nile red per 1 mg of polymer, and all triblock copolymers demonstrated increasing encapsulation efficiency at lower weight ratios of Nile red per polymer. The triblock copolymer, PPS D_{200}-$AD_{20\%}$, yielded the lowest encapsulation efficiency (Figure S24, SI File), which is consistent with the decreased stability observed for NPs composed of triblock copolymers with shorter PDMA block lengths and higher grafting density of AD. The PCL D_{300}-$AD_{20\%}$ triblock

copolymer demonstrated an encapsulation profile comparable to its analog PPS triblock copolymer when Nile red was loaded at a weight ratio of 10 wt% or less.

Small molecule drug release from PPS NPs is triggered by ROS, which converts PPS to its more water-soluble forms of poly(sulfoxide) or poly(sulfone)[11]. To evaluate ROS-responsive release from PPS NP/HA hydrogels, Nile red was loaded into the lead four candidate PPS NP/HA hydrogels, which were then incubated with increasing doses of H_2O_2 (Figure S25, SI File). All PPS NP/HA hydrogels demonstrated release dependent on increasing H_2O_2. Interestingly, PPS NP/HA hydrogels formed at a ratio of 2CD/1AD showed higher cumulative release of Nile red over the same time scale compared to those hydrogels formed at a ratio of 1CD/1AD (Figure S25B and S25D, SI File). The total weight percent of NP/HA hydrogels remained constant (7.5 wt%) in all formulations, there is a higher excess of ROS relative to PPS in hydrogels formed at 2CD/1AD compared to hydrogels formed at 1CD/1AD, which may explain why these hydrogels demonstrate greater cumulative release of small molecule cargo from the core of PPS triblock copolymer NPs.

2.6. PPS-based NP/HA Hydrogels Display Susceptibility to Oxidative and Enzymatic Degradation

Oxidative degradation of PPS D_{300}-$AD_{20\%}$ 2CD/1AD hydrogel compared to both control PCL D_{300}-$AD_{20\%}$ 2CD/1AD and HA/HA 1CD/1AD hydrogels was evaluated by incubating all hydrogels with increasing doses of H_2O_2 and tracking the effect on hydrogel mechanical strength and shear-thinning behavior over time. The G' of all hydrogels demonstrated an H_2O_2-dependent decrease over time (Figure 4A–C). The PPS NP/HA hydrogel surprisingly showed slower degradation in the presence of ROS compared to PCL NP/HA hydrogels and HA/HA hydrogels, with the HA/HA hydrogel demonstrating the most sensitivity to ROS-dependent degradation. Heat maps were also generated to reflect changes in tanδ of hydrogels in response to oxidative degradation (Figure 4D–F). PPS D_{300}-$AD_{20\%}$ hydrogels incubated with 1 mM and 10 mM of H_2O_2 remained in their hydrogel state for up to 48 hours ($\tan\delta < 1$) while incubation with 100 mM H_2O_2 transitioned them to a viscous solution. Control PCL D_{300}-$AD_{20\%}$ hydrogels behaved analogously to PPS counterparts when subjected to 1 mM and 10 mM H_2O_2 but demonstrated a more rapid transition to a viscous solution at 24 hours. Control HA/HA hydrogels exhibited the quickest transition from their hydrogel state to a viscous solution (within 24 hours) compared to the other NP/HA hydrogels across all concentrations of H_2O_2. These results indicate that HA is susceptible to oxidative degradation, which is consistent with the previous literature[27], and furthermore suggests that PPS serves as a “ROS sink” which slows down the oxidative degradation of HA through its consumption of ROS by its own oxidation. These data demonstrate the use of PPS NP/HA hydrogels as promising antioxidant biomaterial that can detoxify ROS in the local tissue microenvironment and protect the HA biopolymer from oxidative degradation. Protecting and increasing local persistence of HA is anticipated to be desirable, as HA is known to be beneficial for tissue repair by maintaining moisture, increasing angiogenesis, stimulating anti-inflammatory pathways, and promoting granulation tissue formation[28–31].

Hyaluronidases are physiologic endoglycosidases that cleave internal beta-N-acetyl-D-glucosaminidic linkages of HA, yielding N-acetylglucosamine and glucuronic acid[28]. Enzymatic degradation of NP/HA hydrogels compared to control HA/HA hydrogels was evaluated by incubating these three hydrogels in the presence of 7 U/mL hyaluronidase, which is within a physiologically relevant range for this enzyme[29], and tracking the effect on hydrogel mechanical strength and shear-thinning behavior over time, in an identical manner described above (Figure 4G–L). While PPS and PCL NP/HA hydrogels gradually degraded over 7 days in the presence of hyaluronidase, HA/HA hydrogels fully degraded within 2 days. These results suggest that the physical crosslinking of HA with the NP component sterically protects HA, and that this effect is more efficient when integrated with ROS-responsive PPS NPs compared to when integrated with PCL NPs.

Hydrogel degradation was also measured in the presence of 7 U/mL hyaluronidase and 1 mM H_2O_2 (Figure 4G–L) to evaluate mechanical degradation of hydrogels under conditions more relevant to the physiological environment. The presence of both ROS and hyaluronidase accelerated the degradation of all hydrogels relative to degradation in the presence of hyaluronidase alone; however, PPS NP/HA hydrogels once again maintained the slowest rate of degradation even under both oxidative and enzymatic conditions. These results were further confirmed by assessing the concentration of uronic acid, a degradation product specific to HA, following incubation of PPS and PCL NP/HA as well as HA/HA hydrogels under oxidative, enzymatic, and both oxidative and enzymatic environments. Increased concentrations of uronic acid were detected in HA/HA hydrogels and PCL NP/HA hydrogels under all degradation conditions when compared to PPS NP/HA hydrogels (Figure S26, SI File). These results further support the hypothesis that PPS NP/HA hydrogels protect the HA polymer when it participates in physical crosslinking with ROS-responsive PPS NPs and may increase its residence in highly inflamed tissue environments *in vivo*.

2.7. PPS-based NP/HA Hydrogels are Cytocompatible and Provide Protection from Cytotoxic ROS

The cytocompatibility of the four lead candidate PPS NP/HA hydrogels was assessed relative to control HA/HA hydrogels, which are cytocompatible biomaterials established by previous literature[20, 30]. The viability of NIH 3T3 fibroblasts in 2D culture was evaluated following 24 hours incubation with an overlay of NP/HA hydrogels. All candidate PPS NP/HA hydrogels maintained a high level of cell viability consistent with the viability of cells incubated with HA/HA hydrogels (Figure 5A). The viability of mouse mesenchymal stem cells (mMSCs) encapsulated within the lead candidate PPS D_{300}-$AD_{20\%}$ 2CD/1AD hydrogel and the control PCL D_{300}-$AD_{20\%}$ 2CD/1AD hydrogel was also evaluated to demonstrate the potential of candidate NP/HA hydrogels as a delivery platform for therapeutic cell types. Both PPS and PCL NP/HA hydrogels shown similar levels of viability of mMSCs following 24 hours of incubation in NP/HA hydrogels compared to mMSCs encapsulated in HA/HA hydrogels (Figure 5B).

To evaluate the antioxidant potential of PPS for protecting encapsulated cells from cytotoxic ROS, mMSCs were encapsulated within the lead candidate PPS D_{300}-$AD_{20\%}$ 2CD/1AD

hydrogel as well as control PCL NP/HA and HA/HA hydrogels and incubated with increasing concentrations of H_2O_2 for up to 24 hours. Increased viability was observed when mMSCs were encapsulated in PPS NP/HA hydrogels compared to mMSCs encapsulated in PCL NP/HA hydrogels and HA/HA hydrogels (Figure 5C). Interestingly, HA/HA hydrogels provided increased viability compared to PCL NP/HA hydrogels but lower viability compared to PPS NP/HA hydrogels. These results were also visualized through live/dead staining (Figure 5D) of hydrogel suspensions with encapsulated cells after 24 hours. The following observations suggest that ROS oxidation of the HA backbone (a previously reported phenomenon[27]) provides antioxidant function to protect encapsulated cells from cytotoxic ROS and that a reduction of HA content in the hydrogel formulation reduces this effect, as observed in for the PCL NP/HA system. The PPS NP/HA group provided the highest overall viability of encapsulated cells, even compared to cell encapsulated in HA/HA hydrogels. These data indicate that PPS NP/HA hydrogels incorporate the antioxidant contributions of both HA and PPS and therefore provide superior protection for therapeutic cells when delivered for tissue repair in the text of highly inflamed pathophysiological scenarios impacted by oxidative stress[32].

2.8. PPS-based NP/HA Hydrogels Demonstrate Degradation, Infiltration, and Resorption in Subcutaneous Mice Model

Following confirmation of *in vitro* cytocompatibility of candidate NP/HA hydrogels, the infiltration and degradation profiles of the four lead candidate PPS NP/HA hydrogels were evaluated *in vivo* through subcutaneous implantation in mice. Histological analysis was performed on explanted NP/HA hydrogels at 7 and 14 days post-implantation (Figure 6A and Figure S27, SI File), though control HA/HA hydrogels were difficult to section likely due to their poor integration with surrounding tissue and/or loss during tissue processing. Three of the four candidate PPS NP/HA hydrogels, as well as the control PCL NP/HA hydrogel, demonstrated significant cellular infiltration which matched the rate of hydrogel degradation and resorption (Figure 6A–B). However, one candidate PPS D_{300}-$AD_{20\%}$ 1CD/1AD hydrogel resulted in the poorest cellular infiltration and the least amount of matrix deposition; this hydrogel also elicited a fibrotic encapsulation response, based on the presence of a thicker layer of collagen surrounding the material (Figure 6A). This may be attributable to the high G′ reported for this candidate PPS NP/HA hydrogel which limits the rate at which cells can tunnel into and remodel this material. However, one of the four candidate hydrogels (PPS D_{300}-$AD_{20\%}$ 2CD/1AD) demonstrated similar mechanical strength to PPS D_{300}-$AD_{20\%}$ 1CD/1AD, as both hydrogels possessed G′ greater than 2000 Pa, but the hydrogel containing more HA (D_{300}-$AD_{20\%}$ 2CD/1AD) resulted in significantly higher rates of cellular infiltration and hydrogel degradation, which were more comparable to the rates observed for the other two PPS NP/HA hydrogels (D_{150}-$AD_{10\%}$ 1CD/1AD and D_{150}-$AD_{10\%}$ 2CD/1AD) (Figure 6B). These results suggest that tuning the balance of HA to the NP component in the overall formulation (while maintaining a constant total weight percent of polymer) can be used to achieve a combination of a stronger hydrogel that is still amenable to cellular infiltration and hydrogel degradation *in vivo*. Overall, these results confirm the biocompatibility of candidate PPS and control PCL NP/HA hydrogels and provide further insights into how mechanical properties and balance

of synthetic and biological components used in hybrid hydrogel formulations to control *in vivo* response[16, 33].

The antioxidant activity of PPS NP/HA hydrogels was also assessed by measuring the level of DNA oxidation of infiltrating cells based on nuclear staining intensity for 8-OHdG (Figure 6C). Infiltrating cells of PPS NP/HA hydrogels showed decreased staining intensity compared to those cells within control PCL NP/HA hydrogels (Figure 6D). Since the mild environment of the subcutaneous implantation model is not characterized by enriched levels of oxidative stress, the increased antioxidant activity of PPS NP/HA compared to PCL NP/HA hydrogels may be anticipated to be even more apparent when NP/HA hydrogels are applied into highly inflamed environments characterized by oxidative stress, such as a chronic skin wounds[34].

3. Conclusions

The following work investigated the formation of a hybrid NP/HA shear-thinning hydrogel, which integrates a biologically-derived polymer, HA, with ROS-responsive, self-assembled NPs through physical crosslinking mediated by guest-host supramolecular chemistry. The robust rheological analysis of eighteen different NP/HA hydrogels revealed that the length of the hydrophilic PDMA block and the grafting density of AD demonstrate synergistic effects which determine the stability of self-assembled NPs as well as the mechanical strength and shear-thinning behavior of the resulting NP/HA hydrogels. While NPs containing a shorter hydrophilic block were limited to lower grafting densities of AD, NPs with a longer hydrophilic block maintained stability at higher grafting densities of AD and yielded NP/HA hydrogels with higher moduli. From this mechanical characterization, four lead candidate PPS NP/HA hydrogels were further characterized *in vitro* to demonstrate small molecule drug loading and release, susceptibility to oxidative and enzymatic degradation, cytocompatibility, cell encapsulation, and protection from cytotoxic ROS. Interestingly, it was observed that both PPS and HA contribute to ROS reactivity and antioxidant function of NP/HA hydrogels. The PPS NP/HA hydrogels demonstrated antioxidant behavior relative to PCL NP/HA hydrogels *in vitro* as well as *in vivo*. Most importantly, the presence of PPS NPs slowed the rate of ROS degradation of HA and therefore is anticipated to prolong local retention of HA *in vivo* relative to NP/HA hydrogels made from more conventional polymers (such as PCL). The *in vivo* characterization of PPS NP/HA hydrogels illustrated that hydrogel degradation, infiltration, and resorption were additionally dictated by interactions between mechanical strength and the amount of HA relative to NP in the hydrogel formulation. The studies summarized above establish NP/HA shear-thinning hydrogels as a new hybrid injectable hydrogel system that integrates synthetic and biologically-active polymers, both of which possess unique antioxidant properties, through guest-host mediated physical crosslinking, and demonstrate that NP/HA hydrogels hold tremendous promise for further development as an injectable delivery platform for small molecule drugs and therapeutic cells in tissue repair applications.

4. Experimental Section

Detailed experimental procedures are provided in the Supporting Information.

Supplementary Material

Refer to Web version on PubMed Central for supplementary material.

Acknowledgments

The funding for current research was provided by the NIH through R01EB028690. DLS, TEM, and SEM measurements were performed using the core facilities of the Vanderbilt Institute of Nanoscale Sciences and Engineering (VINSE) and the Vanderbilt Center for Structural Biology Cryo-Electron Microscopy. Illustrations were created with BioRender.com. The authors thank Dr. Scott Guelcher at Vanderbilt University for allowing the use of a Rheometer for mechanical analysis.

References

[1]. Muir VG, Burdick JA, Chemical Reviews 2020;Correa S, Grosskopf AK, Lopez Hernandez H, Chan D, Yu AC, Stapleton LM, Appel EA, Chemical Reviews 2021;Zhao Y, Song S, Ren X, Zhang J, Lin Q, Zhao Y, Chemical Reviews 2022, 122, 5604. [PubMed: 35023737]

[2]. Zander ZK, Hua G, Wiener CG, Vogt BD, Becker ML, Adv Mater 2015, 27, 6283. [PubMed: 26332364]

[3]. Wandel MB, Bell CA, Yu J, Arno MC, Dreger NZ, Hsu YH, Pitto-Barry A, Worch JC, Dove AP, Becker ML, Nat Commun 2021, 12, 446. [PubMed: 33469013]

[4]. Li J, Mooney DJ, Nature Reviews Materials 2016, 1, 16071.

[5]. Clark AY, Martin KE, García JR, Johnson CT, Theriault HS, Han WM, Zhou DW, Botchwey EA, García AJ, Nat Commun 2020, 11, 114. [PubMed: 31913286]

[6]. You Y, Yang J, Zheng Q, Wu N, Lv Z, Jiang Z, Scientific Reports 2020, 10, 11727. [PubMed: 32678203]

[7]. Voorhaar L, Hoogenboom R, Chemical Society Reviews 2016, 45, 4013. [PubMed: 27206244]

[8]. Puza F, Zheng Y, Han L, Xue L, Cui J, Polymer Chemistry 2020, 11, 2339.

[9]. Li H, Yang P, Pageni P, Tang C, Macromolecular Rapid Communications 2017, 38, 1700109;Du F, Qiao B, Nguyen TD, Vincent MP, Bobbala S, Yi S, Lescott C, Dravid VP, de la Cruz M. Olvera, Scott EA, Nat Commun 2020, 11, 4896. [PubMed: 32994414]

[10]. Gupta MK, Martin JR, Werfel TA, Shen T, Page JM, Duvall CL, Journal of the American Chemical Society 2014, 136, 14896; [PubMed: 25254509] Gupta MK, Martin JR, Dollinger BR, Hattaway ME, Duvall CL, Advanced Functional Materials 2017, 1704107.

[11]. Gupta MK, Meyer TA, Nelson CE, Duvall CL, Journal of Controlled Release 2012, 162, 591. [PubMed: 22889714]

[12]. Napoli A, Valentini M, Tirelli N, Müller M, Hubbell JA, Nature Materials 2004, 3, 183; [PubMed: 14991021] Lee SH, Gupta MK, Bang JB, Bae H, Sung H-J, Advanced Healthcare Materials 2013, 2, 908; [PubMed: 25136729] Poole KM, Nelson CE, Joshi RV, Martin JR, Gupta MK, Haws SLC, Kavanaugh TE, Skala MC, Duvall CL, Biomaterials 2015, 41, 166; [PubMed: 25522975] DeJulius CR, Bernardo-Colón A, Naguib S, Backstrom JR, Kavanaugh T, Gupta MK, Duvall CL, Rex TS, Journal of controlled release : official journal of the Controlled Release Society 2021, 329, 762. [PubMed: 33049330]

[13]. Dollinger BR, Gupta MK, Martin JR, Duvall CL, Tissue Engineering Part A 2017, 23, 1120. [PubMed: 28394196]

[14]. Xu Q, Venet M, Wang W, Creagh-Flynn J, Wang X, Li X, Gao Y, Zhou D, Zeng M, Lara-Sáez I, A S, Tai H, Wang W, ACS Applied Materials & Interfaces 2018, 10, 39494; [PubMed: 30376290] He Z, Xu Q, Newland B, Foley R, Lara-Sáez I, Curtin JF, Wang W, Journal of Materials Chemistry B 2021, 9, 6326. [PubMed: 34304256]

[15]. Appel EA, Tibbitt MW, Webber MJ, Mattix BA, Veiseh O, Langer R, Nature Communications 2015, 6, 6295;Roth GA, Gale EC, Alcántara-Hernández M, Luo W, Axpe E, Verma R, Yin Q, Yu AC, Lopez Hernandez H, Maikawa CL, Smith AAA, Davis MM, Pulendran B, Idoyaga J, Appel EA, ACS Central Science 2020, 6, 1800; [PubMed: 33145416] Bovone G, Guzzi EA, Bernhard S, Weber T, Dranseikiene D, Tibbitt MW, Advanced Materials 2022, 34, 2106941.

[16]. Jons CK, Grosskopf AK, Baillet J, Yan J, Klich JH, Saouaf OM, Appel EA, Advanced Functional Materials 2022, n/a, 2203402.

[17]. Guvendiren M, Lu HD, Burdick JA, Soft Matter 2012, 8, 260.

[18]. Bernhard S, Tibbitt MW, Advanced Drug Delivery Reviews 2021, 171, 240; [PubMed: 33561451] Carlini AS, Cassidy MF, Gianneschi NC, in Peptide Macrocycles: Methods and Protocols (Eds: Coppock MB, Winton AJ), Springer US, New York, NY 2022, p. 427;Scheutz GM, Rowell JL, Ellison ST, Garrison JB, Angelini TE, Sumerlin BS, Macromolecules 2020, 53, 4038;d'Arcy R, Siani A, Lallana E, Tirelli N, Macromolecules 2015, 48, 8108.

[19]. van de Manakker F, Vermonden T, van Nostrum CF, Hennink WE, Biomacromolecules 2009, 10, 3157. [PubMed: 19921854]

[20]. Chen MH, Wang LL, Chung JJ, Kim Y-H, Atluri P, Burdick JA, ACS Biomaterials Science & Engineering 2017, 3, 3146. [PubMed: 29250593]

[21]. Rodell CB, Kaminski AL, Burdick JA, Biomacromolecules 2013, 14, 4125. [PubMed: 24070551]

[22]. Rodell CB, MacArthur JW Jr, Dorsey SM, Wade RJ, Wang LL, Woo YJ, Burdick JA, Advanced Functional Materials 2015, 25, 636. [PubMed: 26526097]

[23]. Ortonne J, Journal of Dermatological Treatment 1996, 7, 75.

[24]. Guimarães CF, Gasperini L, Marques AP, Reis RL, Nature Reviews Materials 2020, 5, 351.

[25]. Zhou C, Hillmyer MA, Lodge TP, Journal of the American Chemical Society 2012, 134, 10365. [PubMed: 22694801]

[26]. Vo AA-O, Doumit MA-OX, Rockwell GA-O.

[27]. Duan J, Kasper DL, Glycobiology 2011, 21, 401. [PubMed: 21030538]

[28]. Cavallini M, Antonioli B, Gazzola R, Tosca M, Galuzzi M, Rapisarda V, Ciancio F, Marazzi M, European Journal of Plastic Surgery 2013, 36, 477.

[29]. Yeo Y, Highley CB, Bellas E, Ito T, Marini R, Langer R, Kohane DS, Biomaterials 2006, 27, 4698; [PubMed: 16750564] Domingues RMA, Silva M, Gershovich P, Betta S, Babo P, Caridade SG, Mano JF, Motta A, Reis RL, Gomes ME, Bioconjugate Chemistry 2015, 26, 1571; [PubMed: 26106949] Seong Y-J, Lin G, Kim BJ, Kim H-E, Kim S, Jeong S-H, ACS Omega 2019, 4, 13834. [PubMed: 31497700]

[30]. Zhu H, Mitsuhashi N, Klein A, Barsky LW, Weinberg K, Barr ML, Demetriou A, Wu GD, Stem Cells 2006, 24, 928; [PubMed: 16306150] Gaffey AC, Chen MH, Venkataraman CM, Trubelja A, Rodell CB, Dinh PV, Hung G, MacArthur JW, Soopan RV, Burdick JA, Atluri P, The Journal of Thoracic and Cardiovascular Surgery 2015, 150, 1268. [PubMed: 26293548]

[31]. West DC, Hampson IN, Arnold F, Kumar S, Science 1985, 228, 1324; [PubMed: 2408340] Moseley R, Walker M, Waddington RJ, Chen WYJ, Biomaterials 2003, 24, 1549. [PubMed: 12559815]

[32]. Zeng W, Xiao J, Zheng G, Xing F, Tipoe GL, Wang X, He C, Chen Z-Y, Liu Y, Scientific Reports 2015, 5, 11100; [PubMed: 26057841] Lai J-Y, Luo L-J, Biomacromolecules 2015, 16, 2950; [PubMed: 26248008] Park JH, Kang S-S, Kim JY, Tchah H, Investigative Ophthalmology & Visual Science 2015, 56, 5614. [PubMed: 26305534]

[33]. Sarem M, Arya N, Heizmann M, Neffe AT, Barbero A, Gebauer TP, Martin I, Lendlein A, Shastri VP, Acta Biomaterialia 2018, 69, 83; [PubMed: 29378326] Wang L, Wang C, Wu S, Fan Y, Li X, Biomaterials Science 2020, 8, 2714. [PubMed: 32307482]

[34]. Ebrahimian TG, Heymes C, You D, Blanc-Brude O, Mees B, Waeckel L, Duriez M, Vilar J, Brandes RP, Levy BI, Shah AM, Silvestre J-S, The American Journal of Pathology 2006, 169, 719; [PubMed: 16877369] Ceradini DJ, Yao D, Grogan RH, Callaghan MJ, Edelstein D, Brownlee M, Gurtner GC, Journal of Biological Chemistry 2008, 283, 10930. [PubMed: 18227068]

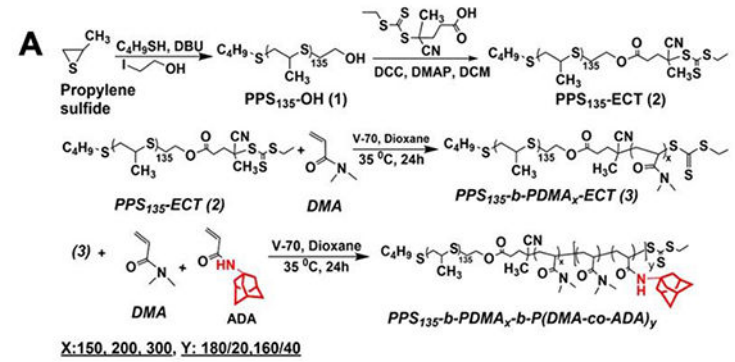

B	Polymer	Abbreviation	MW (Da)[a]
ABC-AD Triblock Copolymers and Precursors	PPS_{135}-OH	PPS_{135}-OH	10,000
	PPS_{135}-ECT	PPS_{135}-ECT	10,260
	PPS_{135}-b-$PDMA_{147}$-ECT	D_{150}	24,770
	PPS_{135}-b-$PDMA_{204}$-ECT	D_{200}	30,460
	PPS_{135}-b-$PDMA_{293}$-ECT	D_{300}	39,270
	PPS_{135}-b-$PDMA_{147}$-b-$PDMA_{188}$-co-ADA_{24}	D_{150}-$AD_{10\%}$	48,150
	PPS_{135}-b-$PDMA_{147}$-b-$PDMA_{165}$-co-ADA_{46}	D_{150}-$AD_{20\%}$	50,220
	PPS_{135}-b-$PDMA_{204}$-b-$PDMA_{176}$-co-ADA_{18}	D_{200}-$AD_{10\%}$	51,410
	PPS_{135}-b-$PDMA_{204}$-b-$PDMA_{167}$-co-ADA_{43}	D_{200}-$AD_{20\%}$	55,490
	PPS_{135}-b-$PDMA_{293}$-b-$PDMA_{184}$-co-ADA_{24}	D_{300}-$AD_{10\%}$	62,250
	PPS_{135}-b-$PDMA_{293}$-b-$PDMA_{164}$-co-ADA_{41}	D_{300}-$AD_{20\%}$	63,590
	PCL_{87}-b-$PDMA_{291}$-b-$PDMA_{167}$-co-ADA_{47}	PCL D_{300}-$AD_{20\%}$	64,920
HA-CD	10%β-CD-g-Hyaluronic acid	HA-$CD_{10\%}$	86,410
	20%β-CD-g-Hyaluronic acid	HA-$CD_{20\%}$	98,120
	34%β-CD-g-Hyaluronic acid	HA-$CD_{34\%}$	116,190

[a]Determined by ^{1}H NMR spectra

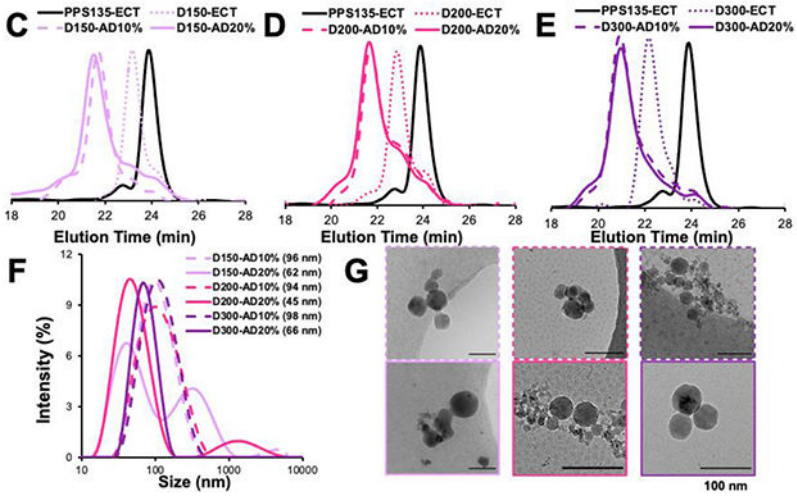

Figure 1. Synthesis of PPS ABC triblock copolymers and self-assembly of NPs.

(**A**) ABC triblock copolymer synthesis involves (1) Synthesis of hydroxy end terminated PPS_{135}-OH by anionic polymerization; (2) Conjugation to create PPS_{135}-ECT RAFT macro–CTA; (3) Synthesis of a diblock copolymer of PPS_{135}-b-$PDMA_x$-ECT by RAFT polymerization of DMA (x = 150, 200, and 300); (4) Synthesis of ABC triblock copolymer of PPS_{135}-b-$PDMA_x$-b-P(DMA-co-$ADA)_y$ from diblock copolymer by RAFT polymerization with y=200 (DMA180/ADA20, and DMA160/ADA40). (**B**) Composition and molecular weight of all polymers synthesized. GPC refractive index detector traces of

(C) PPS_{135}-ECT, PPS_{135}-b-$PDMA_{147}$-ECT, PPS_{135}-b-$PDMA_{147}$-b-P(DMA_{188}-co-ADA_{24}), and PPS_{135}-b-$PDMA_{147}$-b-P(DMA_{165}-co-ADA_{46}); **(D)** PPS_{135}-ECT, PPS_{135}-b-$PDMA_{204}$-ECT, PPS_{135}-b-$PDMA_{204}$-b-P(DMA_{176}-co-ADA_{18}), and PPS_{135}-b-$PDMA_{204}$-b-P(DMA_{167}-co-ADA_{43}); **(E)** PPS_{135}-ECT, PPS_{135}-b-$PDMA_{293}$-ECT, PPS_{135}-b-$PDMA_{293}$-b-P(DMA_{184}-co-ADA_{24}), and PPS_{135}-b-$PDMA_{293}$-b-P(DMA_{164}-co-ADA_{41}). **(F)** DLS hydrodynamic size distribution and (**G)** representative cryo-TEM images of PPS triblock copolymer NPs. All scale bars represent 100 nm.

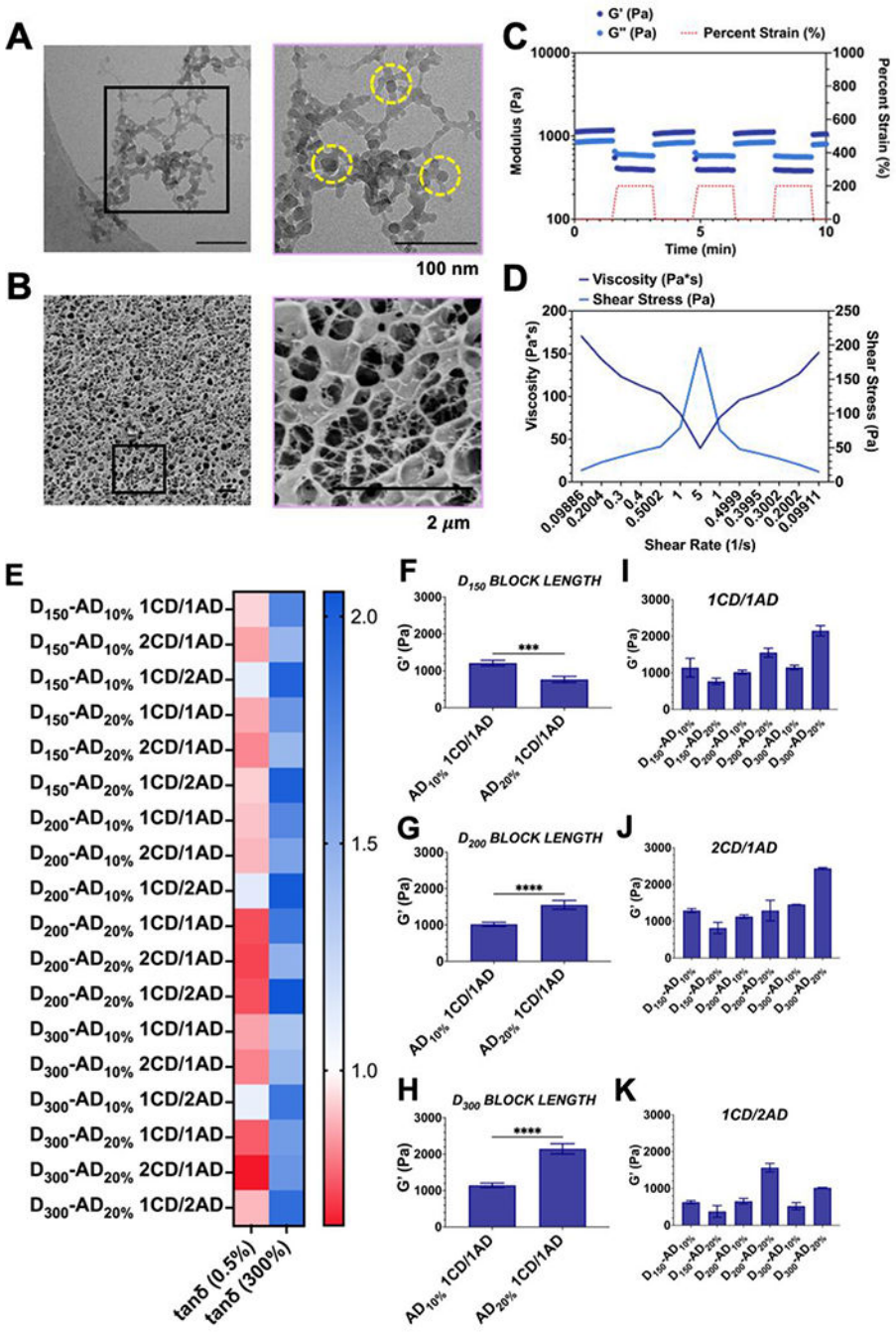

Figure 2. Rheological characterization of PPS NP/HA shear-thinning hydrogel formulations.

PPS NP/HA hydrogels formed by mixing D_{150}-$AD_{10\%}$ with HA-$CD_{20\%}$ (7.5 wt% in PBS) results in stable hydrogels with porous interconnected microstructure captured by (**A**) cryo-TEM imaging (scale bar represents 100 nm) and (**B**) cryo-SEM imaging (scale bar represents 2 μm). Higher magnification of cryo-TEM images (black inset) reveals NPs (yellow circle) embedded within hydrogel matrix. PPS NP/HA hydrogel formulation demonstrates shear-thinning behavior (**C**) in a stepwise percent strain-based time sweep and (**D**) continuous flow measurements. **(E)** Heat map illustrating loss factor (tan δ) of candidate

PPS NP/HA hydrogels (n=3) when subjected to 0.5% and 300% strain. **(F-H)** Effect of AD grafting density in the third block of triblock copolymer on G' of resultant hydrogels (n=3) for triblock copolymers with PDMA block DPs of **(F)** 150, **(G)** 200, and **(H)** 300 units. **(I-K)** G′ for hydrogel formulations as a function of PDMA block DP and grafting density of AD when formulated at CD/AD ratios of **(I)** 1, **(J)** 2, and **(K)** 0.5. All data are presented as means (± s.e.m.). Significance determined as *P < 0.05, **P < 0.01, ***P < 0.001, ****P < 0.0001, and n.s. (not significant) by one-way ANOVA statistical analysis.

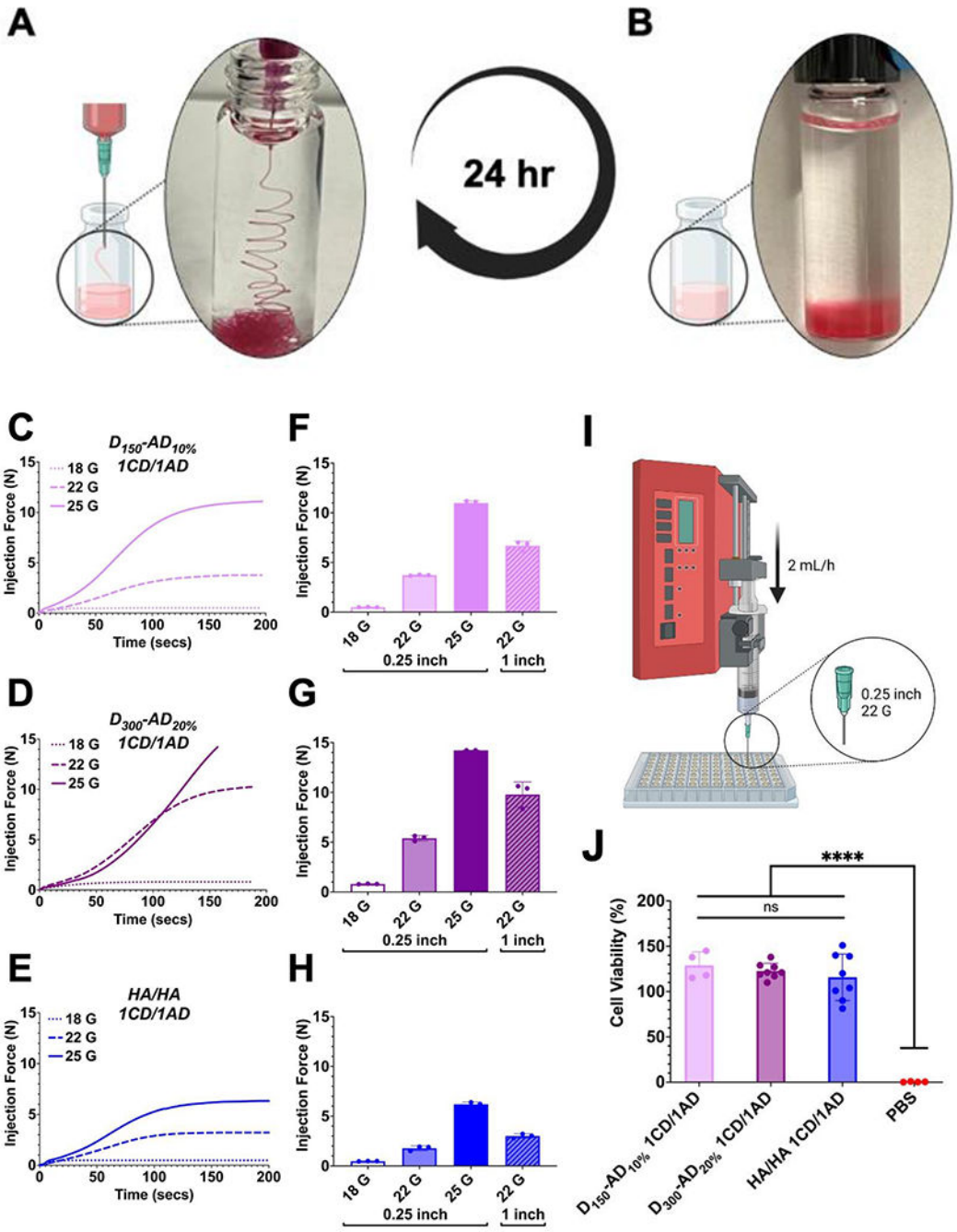

Figure 3. ***In vitro*** **evaluation of PPS NP/HA shear-thinning hydrogels as an injectable delivery platform of therapeutic cells.**

Injection of candidate PPS D_{300}-$AD_{20\%}$ NP/HA 1CD/1AD hydrogel (7.5 wt%) observed when (**A**) hydrogel is injected through 30G needle (0.25 inch length) into PBS without hydrogel dispersion or dilution, and retention and stability is observed when the (**B**) injected hydrogel retains shape in solution without dispersion of dye in PBS for up to 24 hours post-injection. Representative traces of injection force over time for (**C**) PPS D_{150}-$AD_{10\%}$ 1CD/1AD hydrogel, (**D**) PPS D_{300}-$AD_{20\%}$ 1CD/1AD hydrogel, and (**E**) HA/HA 1CD/1AD

hydrogel when injected through needles (0.25 inch length) of varying gauges. Quantification of injection force required to pass the (**F**) PPS D_{150}-$AD_{10\%}$ 1CD/1AD hydrogel, (**G**) PPS D_{300}-$AD_{20\%}$ 1CD/1AD hydrogel, and (**H**) HA/HA 1CD/1AD hydrogel (n=3) through needles (0.25 inch length) of varying gauges (18G, 22G, 25G) and a 25G needle of varying lengths (0.25 inch, 1 inch). Viability of mMSCs following hydrogel encapsulation and injection was evaluated as shown in the diagram (**I**) where injection was performed at a constant flow rate (2 mL/hr) maintained by a syringe pump, and cell viability post-injection was quantified by (**J**) Cell Titer-Glo measurements to compare viability of cells delivered in PPS NP/HA hydrogel, HA/HA hydrogel, or PBS as vehicle (n=8). All data are presented as means (± s.e.m.). Significance determined as *P < 0.05, **P < 0.01, ***P < 0.001, ****P < 0.0001, and n.s. (not significant) by one-way ANOVA statistical analysis.

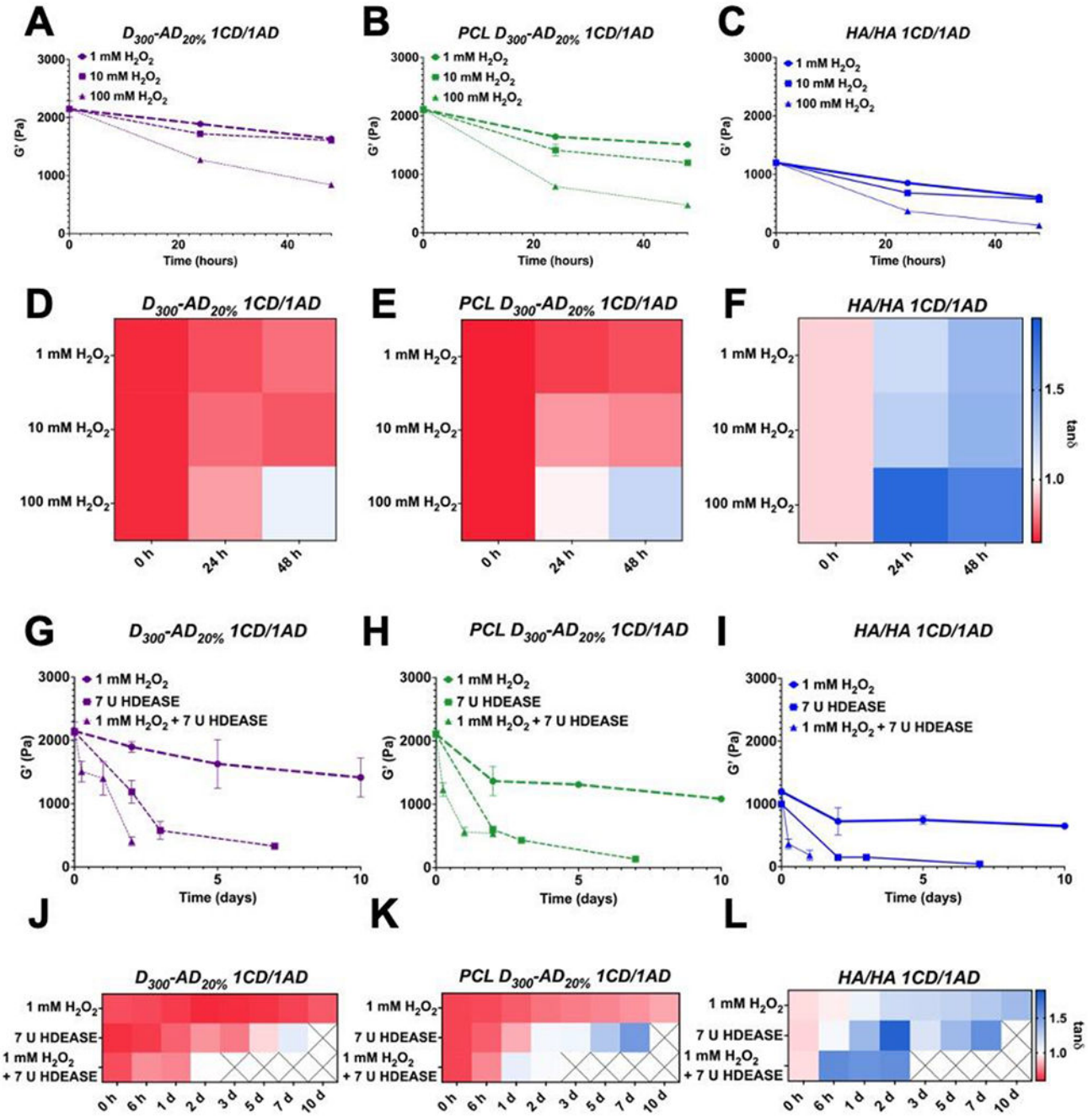

Figure 4. *In vitro* mechanical degradation profiles of PPS NP/HA and control PCL NP/HA and HA/HA shear-thinning hydrogels.

Effect of oxidative degradation on G′ for (**A**) PPS D_{300}-$AD_{20\%}$ 1CD/1AD, (**B**) PCL D_{300}-$AD_{20\%}$ 1CD/1AD, and (**C**) HA/HA 1CD/1AD hydrogels (7.5 wt% PBS) (n=3) when incubated with 1 mM, 10 mM, and 100 mM of H_2O_2 for 48 hours. The corresponding tanδ-based heat map profiles for (**D**) PPS D_{300}-$AD_{20\%}$1CD/1AD, (**E**) PCL D_{300}-$AD_{20\%}$ 1CD/1AD, and (**F**) HA/HA 1CD/1AD (7.5 wt% PBS) (n=3) subjected to 1 mM H_2O_2, 10 mM H_2O_2, and 100 mM H_2O_2 for up to 48 hours. A comparison of oxidative (1 mM

H_2O_2), enzymatic (7 U/mL hyaluronidase), and combined (oxidative (1 mM H_2O_2) plus enzymatic (7 U/mL hyaluronidase)) degradation mediated decrease in G′ of (**G**) PPS based D_{300}-$AD_{20\%}$ 1CD/1AD, (**H**) PCL D_{300}-$AD_{20\%}$ 1CD/1AD, (**I**) HA/HA 1CD/1AD hydrogels (7.5 wt% PBS) (n=3) for up to 7 days. The corresponding tanδ-based heat map profiles for (**J**) PPS based D_{300}-$AD_{20\%}$ 1CD/1AD, (**K**) PCL D_{300}-$AD_{20\%}$ 1CD/1AD, and (**L**) HA/HA 1CD/1AD hydrogels (7.5 wt% PBS) (n=3) subjected to enzymatic, oxidative, and combined oxidative and enzymatic degradation for up to 7 days. All data are presented as means (± s.e.m.).

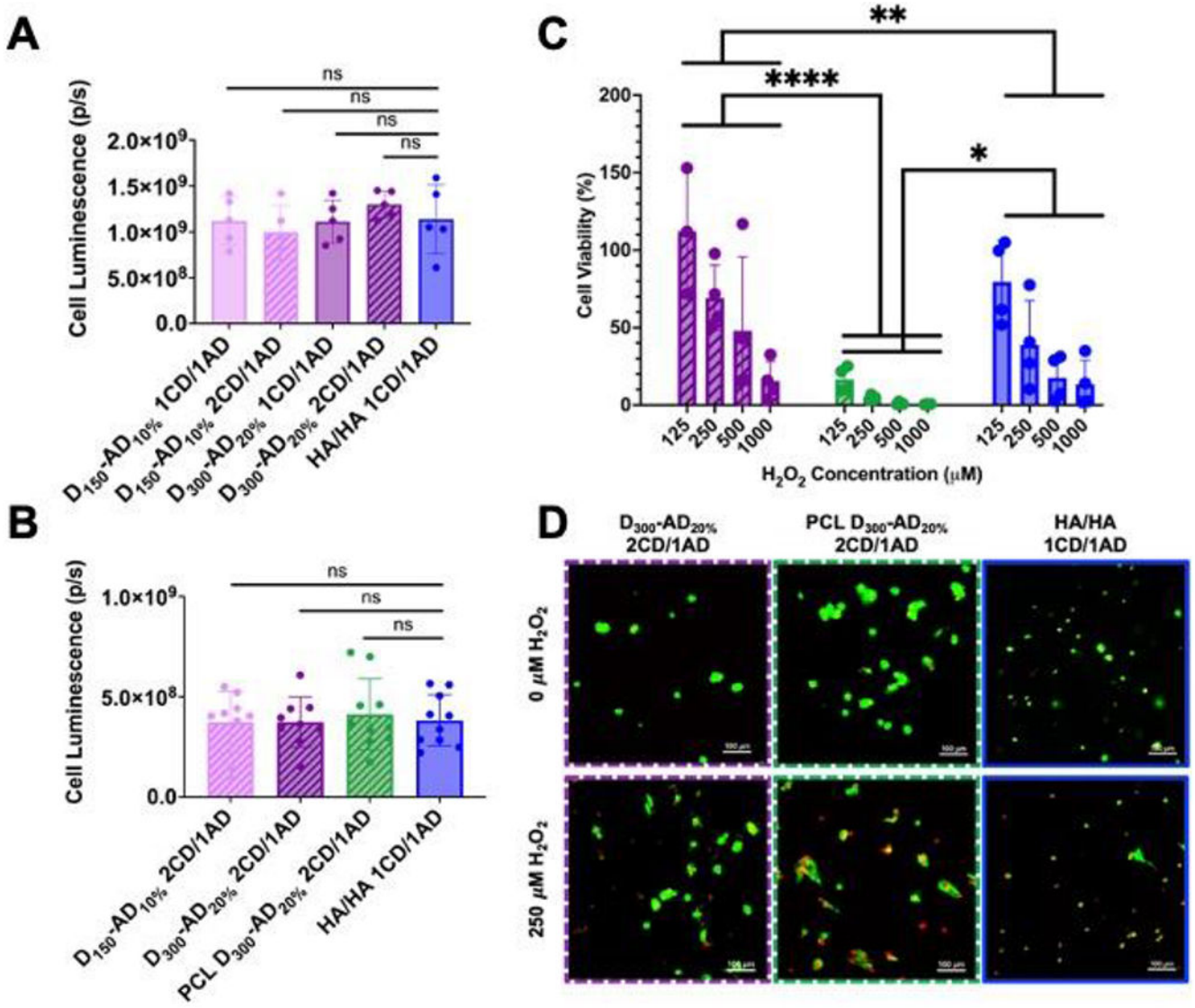

Figure 5. ***In vitro*** **cytocompatibility and cytoprotective capabilities of PPS NP/HA shear-thinning hydrogels.**

Quantification of Cell Titer-Glo measurement of cytocompatibility of PPS D_{150}-$AD_{10\%}$ 1CD/1AD, PPS D_{150}-$AD_{10\%}$ 2CD/1AD, PPS D_{300}-$AD_{20\%}$ 1CD/1AD, and PPS D_{300}-$AD_{20\%}$ 2CD/1AD (7.5 wt% PBS) following (**A**) hydrogel overlay (n=5) on NIH 3T3 fibroblasts in 2D culture and following (**B**) encapsulation of mMSCs in hydrogels (n=8) in 3D culture. Quantification of Cell Titer-Glo measurement of the viability of (**C**) encapsulated mMSCs in PPS D_{300}-$AD_{20\%}$ 2CD/1AD, PCL D_{300}-$AD_{20\%}$ 2CD/1AD, and HA/HA 1CD/1AD hydrogels (7.5 wt% PBS) (n=4-5) in 3D culture and subjected to H_2O_2. (**D**) Representative microscopy images of mMSCs encapsulated within PPS D_{300}-$AD_{20\%}$ 2CD/1AD, PCL D_{300}-$AD_{20\%}$ 2CD/1AD, and HA/HA 1CD/1AD hydrogels (7.5 wt% PBS) and stained by calcein AM (live stain) and ethidium homodimer (dead stain) following 24 hours of incubation with 0 μM or 250 μM of H_2O_2. All data are presented as means (±

s.e.m.). Significance determined as *P < 0.05, **P < 0.01, ***P < 0.001, ****P < 0.0001, and n.s. (not significant) by one-way ANOVA statistical analysis.

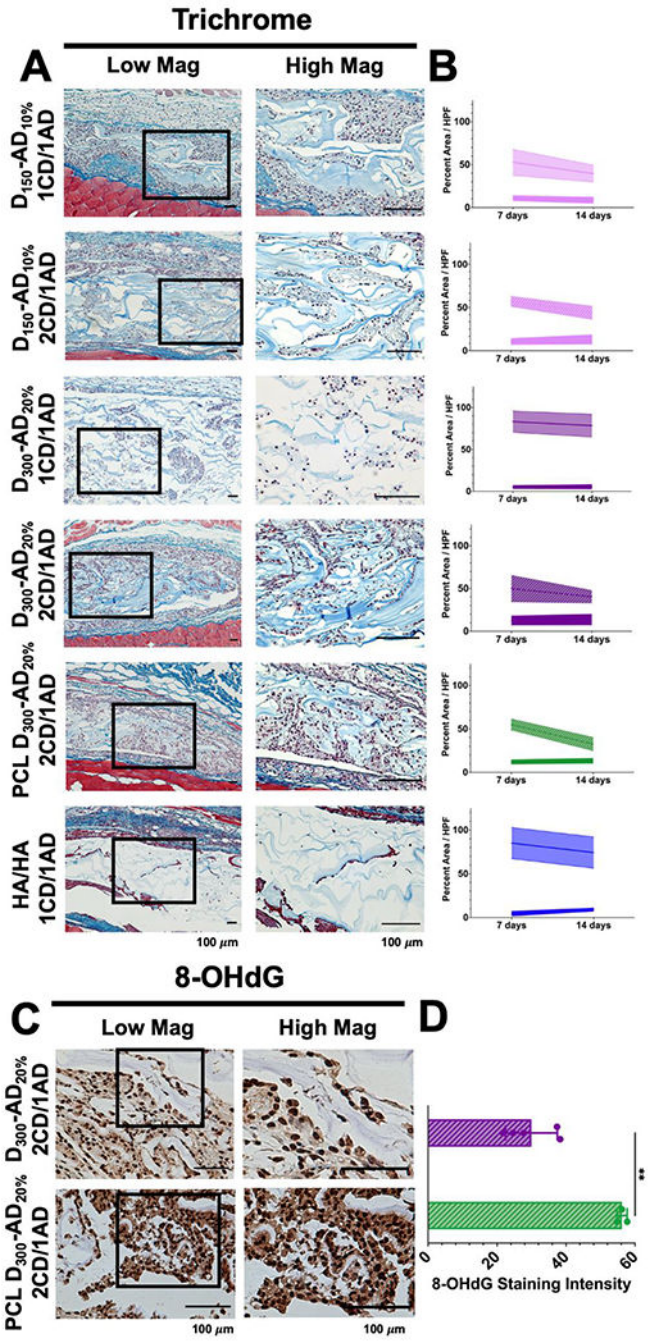

Figure 6. ***In vivo*** **cellular infiltration and material resorption of PPS NP/HA shear-thinning hydrogels in a subcutaneous mouse model.**

(**A**) Representative Masson's trichrome stained explanted hydrogel sections at day 7 post-implantation. All scale bars represent 100 μm. Voids in histology for D_{300}-$AD_{20\%}$ 1CD/1AD and HA/HA 1CD/1AD reflect loss of gels during processing/sectioning due to the poor cell and matrix integration with these hydrogels. Histological quantification of excised gel/tissue sections demonstrates (**B**) timecourse of cellular infiltration (bottom shaded curve) and hydrogel degradation (top patterned curve) quantified for each hydrogel implanted subcutaneously (n = 5). Data are presented as means (± s.e.m.). Immunohistochemical

characterization of DNA oxidation of cells by (**C**) representative 8-OHdG IHC stained sections for PPS NP/HA and control PCL NP/HA hydrogels at day 7 post-implantation. All scale bars represent 100 μm. Quantification of 8-OHdG positive nuclei in excised gel/tissue sections demonstrates (**D**) reduced staining intensity for 8-OHdG in infiltrating cells of candidate PPS NP/HA hydrogels (n=5) compared to those cells infiltrating PCL NP/HA hydrogels (n=3). Data are presented as means (± s.e.m.). Significance determined as *P < 0.05, **P < 0.01, ***P < 0.001, ****P < 0.0001, and n.s. (not significant) by two-tailed Student's t-test.